

Synthesis and characterization of Ge nanocrystals embedded in high-k dielectric (HfO₂) matrix

V. Saikiran^{1*}, N. Manikanthababu¹, N. Srinivasa Rao², S. V. S. Nageswara Rao¹, A. P. Pathak¹

¹*School of Physics, University of Hyderabad, Hyderabad 500046, India*

²*Department of Physics, Malaviya National Institute of Technology, Jaipur 302017, India*

*Corresponding author. E-mail: saivadavalli@gmail.com; sai_vadavalli@yahoo.com

Received: 06 January 2016, Revised: 18 June 2016 and Accepted: 22 June 2016

ABSTRACT

Trilayered HfO₂/Ge/HfO₂ thin films were grown on Si substrate by RF magnetron sputtering with HfO₂ and Ge targets. The subsequent rapid thermal annealing (RTA) of these films at 700 & 800°C results in formation of Ge nanocrystals (NCs) in HfO₂ matrix. X-ray diffraction (XRD) and micro-Raman spectroscopy measurements were performed to confirm the formation of Ge NCs in the annealed samples. XRD results indicate that the as-deposited samples show amorphous behaviour, whereas the annealed samples clearly confirm the crystallinity of the films. The average size of the Ge NCs was found to increase with an increase in annealing temperature. Raman scattering studies confirm that the annealed samples exhibit a shift in peak position corresponding to Ge-Ge optical phonon vibrations, which clearly indicates the formation of Ge NCs. Conversely, as-deposited samples were also irradiated with swift heavy ions of 150 MeV Au and 80 MeV Ni at a fluence of 3×10^{13} ions/cm² to synthesize Ge NCs. The structural properties of pristine and irradiated samples have been studied by using X-ray diffraction, Raman spectroscopy to substantiate the growth of Ge NCs upon irradiation. The results obtained by RTA are compared with the irradiated ones. Copyright © 2016 VBRI Press.

Keywords: Ge nanocrystals; high-k dielectric HfO₂; XRD; micro-raman; ion irradiation.

Introduction

IC technology is on a constant look out for potential materials to replace SiO₂ for further optimization of device fabrication. The thickness of SiO₂ layer has reached its fundamental material limitation beyond which the leakage currents leading to detrimental effects in device operation. HfO₂ is one of the most promising materials for possible replacement of SiO₂ due to its higher dielectric constant and feasible larger oxide thickness corresponding to the same level of capacitance as achieved for a thinner SiO₂ dielectric layer [1, 2]. HfO₂ has also been treated as a useful material in flash memory applications owing to its large charge storage capacitance [3, 4]. Nanocrystals embedded in such a dielectric matrix as HfO₂ have potential applications in integrated flash memory devices. The uses of NCs as floating gate memories offer smaller operating voltages and faster write/erase speeds when compared to conventional flash memories [5-7]. It is well known that the semiconductors as well as metals (Si [8], Ge [9], SiGe [10], Ni [11], Au [12] and Ag [13]) have been considered as capable materials for the charge storage nodes in nanocrystal-based floating flash memory devices. Si and Ge NCs are regarded as ideal candidates for memory applications because of their small band-gap, high carrier mobilities and large Bohr exciton radius in comparison with the metal NC based devices. Due to their effective masses

and energy differences between Si and Ge; the Ge NCs are technologically more advantageous than Si NCs [14]. Moreover, the Bohr exciton radius of Ge (24 nm) is much larger than that of Si (5 nm), which indicates that the quantum confinement effects are more prominent in Ge NCs [15]. Also, Ge has excellent band offset values with longer retention time compared to Si. Thus, Ge NCs based materials have garnered considerable attention as a promising candidate for charge storage applications in non-volatile memory devices [16]. The studies on the formation and growth of Ge NCs embedded in SiO₂ [17-20] are well known whereas such studies on Ge NCs embedded in HfO₂ are limited [21]. There are very few reports available on the formation and growth kinetics of Ge NCs in HfO₂ matrix [22]. These NCs embedded in a high-k dielectric matrix such as HfO₂ will certainly improve the performance of the memory devices. Hence, in recent times, Ge NCs embedded in HfO₂ dielectrics have been considered for the memory applications [23]. In order to fabricate Ge NCs in HfO₂ based devices, the crystallization kinetics of Ge NCs embedded in the high-k dielectric matrix are to be well-understood as they possess important applications in memory devices [21-23].

In general, the formation of NCs embedded in a dielectric matrix includes the deposition of thin films by a physical deposition method and then followed by high temperature annealing. The growth and formation of NCs in HfO₂

matrix and the interface effects of Ge/HfO₂ during the formation are to be understood. During the process of Ge NCs synthesis by annealing at high temperatures, the formation of GeO or HfGeO related phases maybe possible. So the understanding of the phenomena of growth and formation of Ge NCs is very important. Ion beam irradiation is established as an interesting tool in the synthesis and modification of embedded NCs. Swift heavy Ion (SHI) irradiation is an established method for the formation of Ge NCs in the as-deposited amorphous Ge samples by ion beam induced annealing [24, 25]. It is well known that during SHI irradiation process, ion beam mixing in semiconductor and dielectric layers can occur and form a mixed state [26, 27]. Also, ion irradiation induced modification of embedded NCs is well studied [28-30]. However, there are no reports available on the formation of HfGeO or HfGeO_x during SHI irradiation of Ge/HfO₂ layers, but few reports have been found on the ion beam synthesis of Ge NCs in HfO₂ by low energy ion implantation followed by annealing [31, 32]. The synthesis of Ge NCs embedded in HfO₂ matrix by high energy irradiation reported here is one the first of its kind in ion beam synthesis.

Here we report the synthesis of Ge NCs embedded in HfO₂ and exploring the formation and growth kinetics of Ge NCs in HfO₂ matrix. Trilayered HfO₂/Ge/HfO₂ films were deposited on Si substrate by RF sputtering. The as-deposited samples were annealed using RTA at various temperatures to synthesize Ge NCs in HfO₂. XRD and micro-Raman spectroscopy measurements have been employed to confirm the formation of Ge NCs in the annealed samples. SHI irradiation has also been used as an alternative method for the formation of Ge NCs in the as-deposited samples. The role of SHI induced annealing effects on the possible formation of Ge NCs in HfO₂ matrix has been studied.

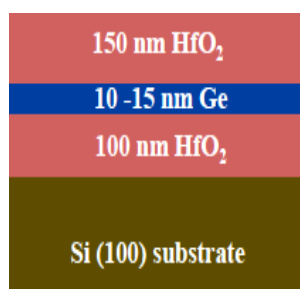


Fig. 1. Schematic of the as deposited HfO₂/Ge/HfO₂ sample.

Experimental

The Tri-layered HfO₂/Ge/HfO₂ thin films were synthesized on a p-type Si (100) substrate at room temperature by RF magnetron sputtering of 99.999 % purity HfO₂ and 99.999 % purity Ge targets. The Si substrates were cleaned with acetone, isopropyl alcohol and deionized water before loading into the deposition chamber. The sputtering was performed with Ar gas. The base pressure for deposition was set at 5x10⁻⁶ torr and the working pressure was maintained at 4.2x10⁻³ torr during the deposition. The schematic of the as deposited sample is shown in Fig. 1.

The as-deposited samples were annealed through a rapid thermal annealing process at 700 and 800°C for 120 s in N₂ atmosphere (1500 SCCM) in order to form the Ge nanocrystals in HfO₂ dielectric matrix.

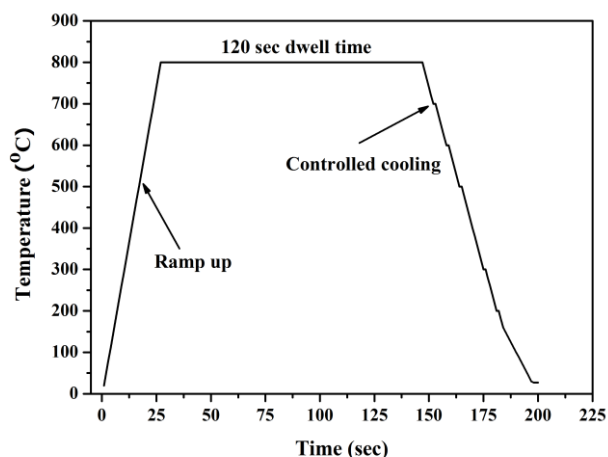


Fig. 2. Typical annealing profile of RTA.

The typical RTA profile is seen in Fig. 2. On the other hand, the as-deposited samples were also irradiated with swift heavy ions of 150 MeV Au and 80 MeV Ni at a fixed fluence of 3x10¹³ions/cm² as an alternative approach to induce the formation of Ge NCs in HfO₂ matrix. The energy losses as well as the ranges of the incident ions inside Ge and HfO₂ systems were calculated using Stopping and Ranges of Ions in Matter (SRIM) simulation code, and the values are given in Table 1. Irradiation was performed in a high vacuum chamber at the pressure < 10⁻⁶ torr.

Table 1. The values of energy losses and projected ranges of incident ions in Ge ($\rho = 5.35$ g/cm³) and HfO₂ ($\rho = 9.7$ g/cm³).

Incident ion	Energy (MeV)	Electronic energy loss (keV/nm)		Nuclear energy loss (keV/nm)		Range (μ m)	
		HfO ₂	Ge	HfO ₂	Ge	HfO ₂	Ge
Au	150	31.8	22.22	0.272	0.492	9	13.6
Ni	80	15.77	10.95	0.024	0.042	8.2	12.4

The samples were scanned over 1cm x 1cm area with the ion beam and a constant current of 1 pA (particle nano-Amp) was maintained throughout the irradiation process. The formation and growth of Ge NCs was studied by using XRD and Raman scattering measurements. XRD measurements were carried out in glancing angle incidence mode with an incidence angle of 1° using a Cu K α source (1.5406 Å). The Raman scattering measurements were carried out at room temperature in backscattering mode using 514.5 nm line of an Ar laser as an excitation source. RBS has been employed to estimate the composition of Ge and HfO₂ in the as-deposited sample. FESEM was used for the morphology of the cross section of the multi-layered thin films. Atomic force microscopy (AFM, Instrument SPA 400 of SPI 3800, Seiko Instruments) has been used to study the surface morphology and the RMS roughness of the as deposited, RTA treated and SHI irradiated samples. More details about the instruments used for different characterizations can be found in our previous papers [33].

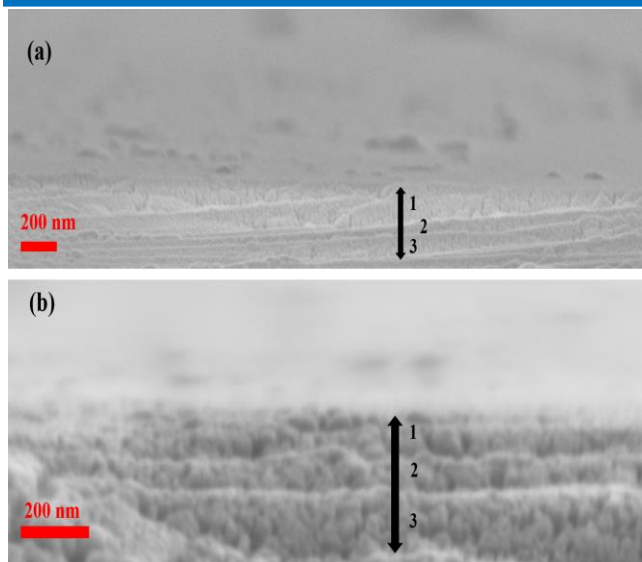


Fig. 3. Cross sectional SEM images of the asdeposited HfO₂/Ge/HfO₂ multilayer thin film.

Results and discussion

The Cross sectional FESEM images of the tri layered samples are shown in **Fig. 3(a, b)**, which give a direct evidence for the multilayer structure of the as deposited samples. After annealing we have observed that a mixed structure and the morphology of the trilayered film mostly disappear and a single layer of HfO₂ with embedded Ge nanocrystals remains. **Fig. 4** shows the RBS spectrum of as-deposited sample. The sample stoichiometry was estimated by the simulation of the spectrum using the SIMNRA code. The Ge composition in the as deposited sample is determined to be about 6 at%. The corresponding Ge, Hf and O edges in the spectra are indicated in the **Fig. 4**. It is clear from the gap in the two peaks of HfO₂ that the Ge is in between the two HfO₂ layers.

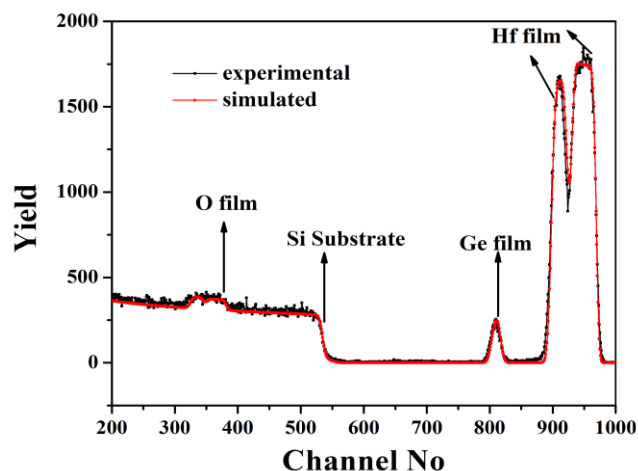


Fig. 4. RBS spectrum of the as-deposited sample.

The diffraction patterns of the as-deposited, RTA treated multilayer samples are presented in **Fig. 5(a)**. In case of the as-deposited sample, no noticeable peak is observed, whereas the RTA sample at 700°C and 800°C show various

diffraction peaks corresponding to Ge (111), (220) and (311) planes. Apart from crystalline Ge peaks the pattern of RTA 800°C sample also has few more peaks at 2θ values 30.66°, 33.43°, 34.75°, 40.21° and 49.55° which indicate the crystalline HfO₂.

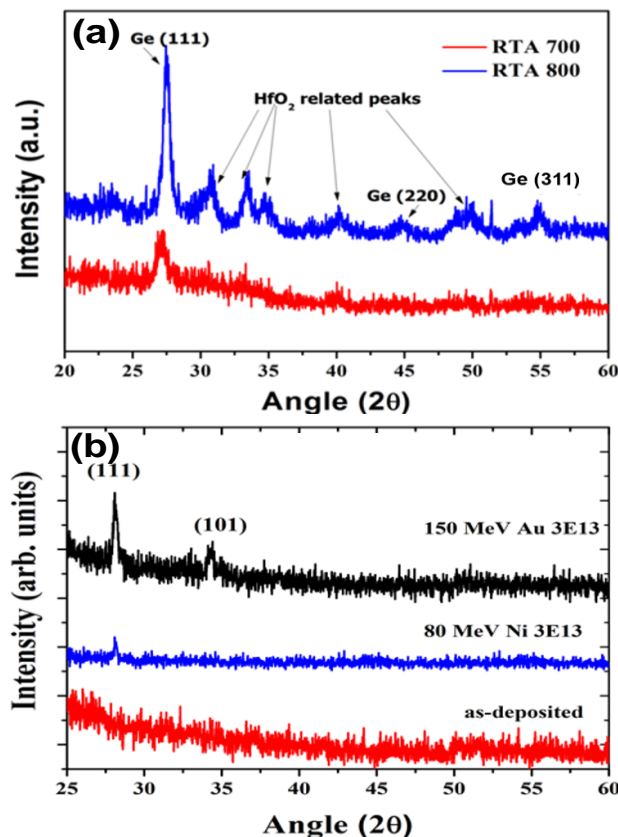


Fig. 5. XRD pattern of the asdeposited, (A) RTA treated and (B) SHI irradiated samples.

These peaks may be attributed to either HfO₂ or an intermediate state of Ge and HfO₂. The RTA 700 °C sample has also some of these peaks, which indicates the early stage of crystallization upon annealing. During the RTA process at high temperature, Ge atoms distributed in the as-deposited sample get higher mobility and crystallize by combining with few more atoms to form a bigger nanocrystal. These Ge NCs were formed by diffusion of Ge atoms or clusters.

Table 2. Variation of Ge NC size for various samples.

Sample	Ge NC size (nm)
AD	-
RTA 700	11
RTA 800	16
Au 3E13	12
Ni 3E13	9

As observed from the figure, XRD peak becomes sharper and the full width at half-maximum (FWHM) of the peak is also reduced with the increase of annealing temperature.

This indicates that the average size of Ge NC increases with annealing temperature. The measured NC sizes using scherrer's formula are given in **Table 2**. With the increase of annealing temperature, Ge atoms and small nanocrystals get higher mobility and diffuse through the dielectric matrix to agglomerate into bigger NCs. The crystallinity of NCs also improves with the increase of annealing temperature as seen from the decrease in FWHM and an increase in intensity of the XRD peaks. In our earlier work on the synthesis of Ge NCs embedded in SiO₂ [17, 29] matrix we have observed only the peaks corresponding to Ge NCs whereas here we have observed some additional peaks due to HfO₂ in the XRD results. The above observation is attributed to the crystallization temperature of HfO₂ is lower than SiO₂. **Fig. 6** shows the diffraction pattern of the only HfO₂ film annealed at 800 °C using RTA. It clearly shows the polycrystalline nature of the pure HfO₂ with different peaks at their respective positions of 2 θ values.

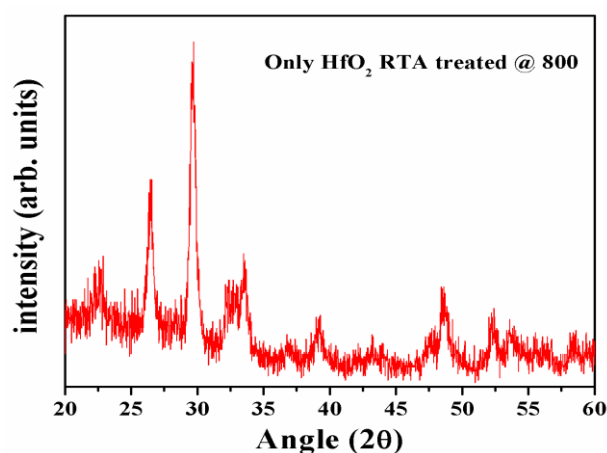


Fig. 6. XRD pattern of the RTA treated sample of only HfO₂ indicates the polycrystalline nature of HfO₂ (JCPDS # 34-0104).

The as-deposited samples were irradiated with swift heavy ions of 150 MeV Au and 80 MeV Ni at a fixed fluence of 3×10^{13} ion/cm² as an alternative approach to synthesize Ge NCs through ion beam irradiation induced annealing. The XRD pattern of the SHI irradiated samples is presented in **Fig. 5(b)**. It is observed that the SHI irradiated samples show diffraction peaks which corresponds to crystalline Ge while the as-deposited sample is amorphous and has no peaks. It indicates that the SHI irradiation is inducing the formation of Ge NCs in trilayered HfO₂/Ge/HfO₂ samples. The NC sizes measured are given in **Table 2**. The energy deposited by 150 MeV Au ions in both Ge and HfO₂ is larger than the energy deposited by 80 MeV Ni ions. Hence the crystallinity improves and the NC size also increases in case of Au irradiation because of the more deposited electronic energy. As a complementary characterization technique, we performed Raman scattering measurements to identify the presence of Ge-Ge bonds and their evolution with respect to annealing.

Fig. 7(a) shows the Raman spectra for as grown and RTA treated samples. As expected Ge-Ge peak located at 300 cm⁻¹ emerged in the spectra after annealing at 700 °C and 800 °C. We have observed that the peak intensity is

low for the sample annealed at 700 °C, and increases with increasing temperature. This is clearly a result of the increase in Ge crystallinity with the temperature. One further feature observed in the Raman spectra is the shift in the peak position: the RTA 700 sample has the Ge-Ge peak at 298 cm⁻¹ whereas the RTA 800 sample had the peak centred at 300 cm⁻¹. This shift of peak position towards the lower wave number side of the sample annealed at 700 °C has been attributed to quantum size effects. It confirms that the size of the NCs in RTA 700 sample is smaller than the size in RTA 800 sample i.e. with the increase in annealing temperature the NC size increases. The annealing temperature of 700 °C is at lower end of the temperature range in which Ge crystallization occurs. We would then expect the sample to have been partially crystallized at this temperature and have an improved crystallinity with increase in temperature.

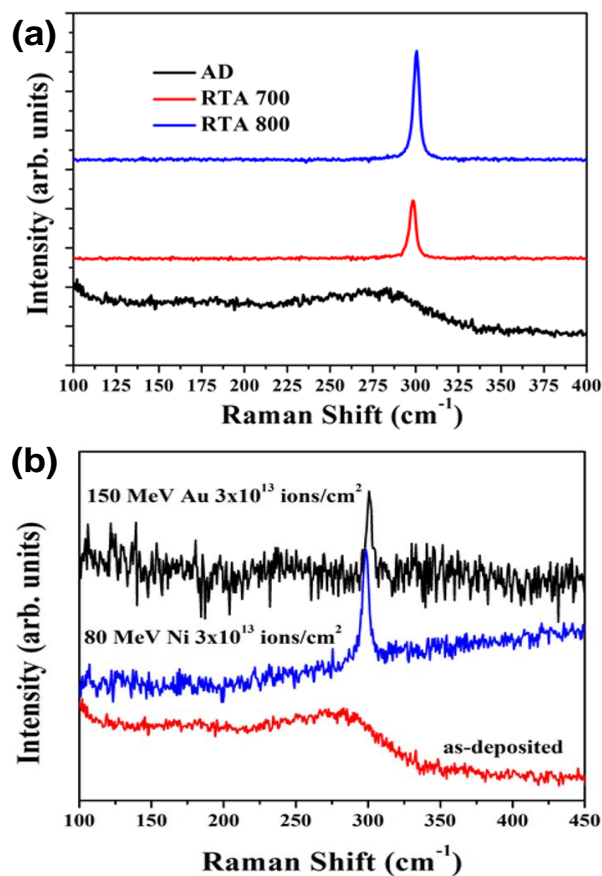


Fig. 7. Raman spectra of the as-deposited, RTA treated and SHI irradiated samples.

As the temperature increases the FWHM of the peak also decreases, which also indicates that the size of the NC increases with the annealing temperature. For the first order Raman spectrum [34-36], we have

$$I(\omega) = \int_0^1 \frac{1 - \frac{q^2 d^2}{4a^2}}{((\omega - \omega(q))^2 + \frac{\Gamma_0^2}{2})} dq \quad (1)$$

$$\omega^2(q) = A + B \cos\left(\frac{\pi q}{2}\right) \quad (2)$$

where, $\omega(q)$ is the phonon dispersion relation, Γ_0 is the natural line width (FWHM) of the scattered signal, and $C(0, \vec{q})$ is the Fourier transform of the phonon confinement, its value depending on the crystallite size. By using the above equations and considering the downshift of the Raman peak and the peak broadening with respect to the bulk Ge, the average size of the NCs can be estimated. The equation that relates the peak shift with the NP size can be given after simplification as,

$$\Delta\omega = \omega(q) - \omega_0 = -A \left(\frac{a}{d}\right)^\gamma \quad (3)$$

where, the values are A and γ are constants and a is the lattice parameter of Ge (0.5658 nm). No peak around 440 cm^{-1} which corresponds to GeO_2 phase has not been observed so it is confirmed that the pure Ge NCs are observed due to annealing of the as deposited samples. **Fig. 7(b)** shows the Raman spectra of the SHI irradiated samples. It is observed that after the SHI irradiation the Ge-Ge optical phonon peak becomes sharper whereas the un-irradiated sample has a broad peak at 270 cm^{-1} . It can also be seen that the peak position of Ge NCs, shifts towards the lower wavenumber side as the irradiation fluence increases. The values of Ge NCs peak position, the shift of respective peaks, and change in the FWHM of the peak for various fluences of all the samples are given in **Table 3**.

Table 3. Ge NCs peak position from Raman spectrum, its peak shift and change in FWHM of the peak for various samples.

S.No	Sample Details	Ge NCs peak position (cm^{-1})	Shift in the peak position from its bulk value (cm^{-1})	FWHM of the Ge NCs peak (cm^{-1})
1	As deposited	270 (broad one)	-	-
2	RTA 700	298	3	4.2
3	RTA 800	300	1	3.8
4	150 MeV Au 3E13	300	1	3.2
5	80 MeV Ni 3E13	298	3	5.2

Ion irradiation effects

Since the dielectric constant and the crystallization temperature of the SiO_2 and HfO_2 are different, so one can expect that during annealing at high temperatures, the formation of GeO or HfGeO related phases maybe possible in Ge- HfO_2 system which were not common in Ge- SiO_2 . The ion irradiation in semiconductor and dielectric layers can lead to a mixed state due to ion beam mixing at high fluences. But up to now there are no reports available on the formation of HfGeO or HfGeO_x during SHI irradiation of Ge/ HfO_2 layers. Here we observed the formation of Ge NCs embedded in HfO_2 matrix. One can explain the basic mechanism of crystallization and formation of nanocrystals in these samples, under ion-irradiation with the help of thermal spike model [37].

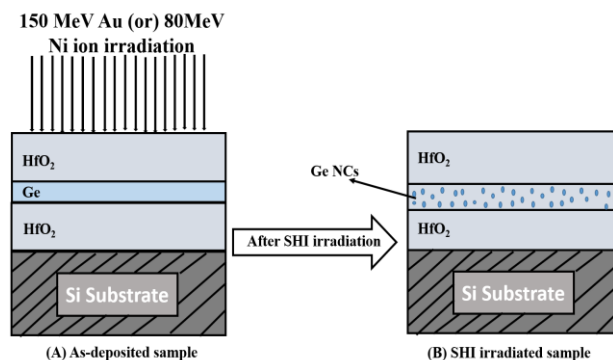


Fig. 8. Schematic representation of the SHI irradiation process of $\text{HfO}_2/\text{Ge}/\text{HfO}_2$ trilayered films deposited on Si substrate.

When the swift heavy ion passes through the matter, it loses energy via electronic energy loss (S_e) and nuclear energy loss (S_n). The swift energy transfer excites the system and the region where the energy is deposited gets suddenly heated to a very high temperature. The material then, gets modified and transforms to the molten state for a short duration. Thus a large amount of energy is transferred to the target leading to an increase of the lattice temperature above its melting point along the ion path. Eventually, the energy is transferred to the target lattice via electron-phonon coupling. The passage of 150 MeV Au and 80 MeV Ni ions deposit the electronic energy (S_e) of the order of 31.8 keV/nm and 15.8 keV/nm respectively, in HfO_2 and similarly 22 keV/nm and 11 keV/nm respectively, in Ge. This energy results in local amorphization and the liberated Ge atoms diffuse inside HfO_2 and agglomerate to crystallize as Ge NCs. As the 150 MeV Au also deposits a reasonable amount of S_n in both HfO_2 and Ge, so the damage creation is also more in the Au irradiated samples compared to the Ni irradiated ones. The same has been observed in the Raman spectra of the Au irradiated sample which is seen as a shoulder peak at 240 cm^{-1} . This is due to the vibrational motion of the oxygen related defects in HfO_2 [38] formed as a result of 150 Au ions irradiation. It has been observed that the size of the Ge NCs in 150 MeV Au irradiated sample is larger than the size of the ones in 80 MeV Ni irradiated at the same fluence, because the growth of the NCs is governed by the deposition of S_e and Au ions deposit more S_e than Ni ions. The schematic representation of the SHI irradiation process is shown in the **Fig. 8**. It will be interesting to see the effects of increase in ion fluence on the growth and modification of Ge NCs. It may be possible to tune the size and properties of Ge NCs by choosing the appropriate energy and ion fluence. From our earlier studies on Ge NCs embedded in SiO_2 matrix it was observed that the SHI irradiation can be used for the synthesis of Ge NCs by varying fluence and energy deposited by irradiating ions inside Ge- SiO_2 films [39]. It can be possible to tune the size and properties of the Ge NCs to some extent under ion irradiation.

AFM surface topographies of the different samples are depicted in **Fig. 9**. From these images only a difference in surface roughness of the different samples has been observed. With increase in fluence of irradiation it was observed that the surface of the samples becomes smoothed

and the particles/grain type morphology disappears from the as-deposited sample. It is observed that the surfaces of the samples become smooth and some self-organized surface structures are observed [40-42]. Though some smooth structures are observed after ion irradiation, more detailed studies are needed to come to a conclusion for the understanding of the surface engineering of HfO₂ surfaces with ion beams. Whereas the annealed samples show different morphology that they retain the particle type nature after the annealing. It was observed that the particle size decreases and the surface roughness more or less remains the same after annealing. The same is observed in the case of only HfO₂ sample also. So it is concluded that the ion beam induced surface smoothing is observed after irradiation with different ions and RTA gives the reduced particle size with no change in the surface roughness.

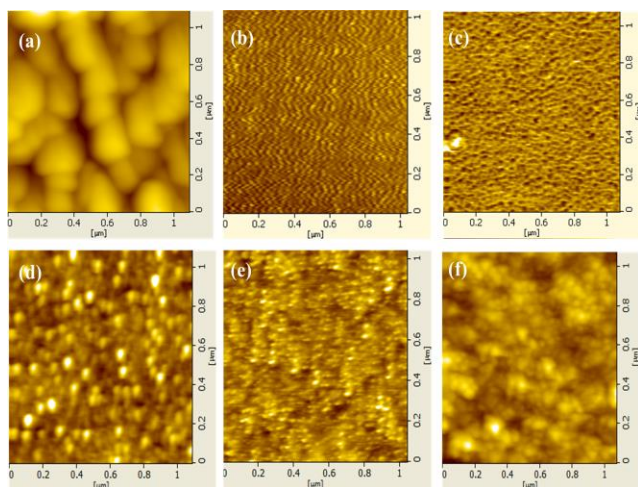


Fig. 9. AFM micrographs of the asdeposited, SHI irradiated and RTA treated samples of HfO₂/Ge/HfO₂, (a) asdeposited, (b) 150 MeV Au 3E13, (c) 80 MeV Ni 3E13 fluence irradiated, (d) RTA 700°C and (e) RTA 800°C annealed. (f) is for the only HfO₂ annealed at 800°C using RTA.

Conclusion

Tri-layered HfO₂/Ge/HfO₂ thin films were synthesized on Si substrate and the as-deposited samples were annealed using RTA at various temperatures. XRD and micro-Raman spectroscopy measurements were carried out to confirm the formation of Ge NCs in the annealed samples. XRD results reveal the formation of crystalline structure in the annealed samples while the as-deposited samples are amorphous in nature. The average size of the Ge NCs is found to increase with increase in the annealing temperature. According to micro-Raman spectra, the annealed samples exhibit a shift in the peak corresponding to Ge-Ge optical phonon vibrations, which clearly indicates the formation of Ge NCs in HfO₂ matrix. SHI irradiation has been used as an alternative method for the formation of Ge NCs in the as-deposited samples and the XRD and micro-Raman Spectroscopy measurements suggest the presence of Ge NCs in the ion irradiated samples. The formation of Ge NCs in HfO₂ matrix as a result of ion irradiation has been understood based on the S_e deposited by incident ion. This process is also called as ion beam induced annealing.

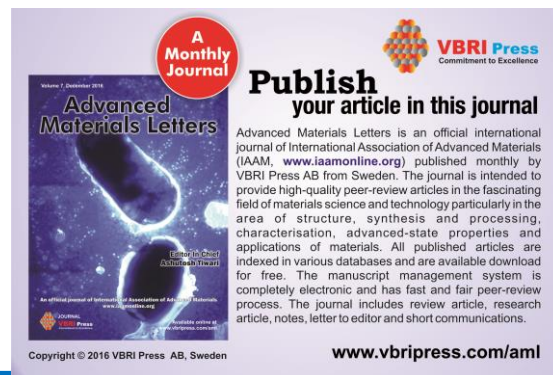
Acknowledgements

APP thanks CSIR-India for Emeritus Scientist award.

References

- Doyle B.; Arghavani R.; barlage D.; data S.; Doczy M.; Kavalieros J.; Murthy A.; and chau R.; *Intel technology, J.* **2002**, *6*, 42.
ISSN: 1535864X
- Wilk G. D.; and Wallace R. M.; *Appl. Phys. Lett.* **1999**, *74*, 2854.
DOI: [10.1063/1.124036](https://doi.org/10.1063/1.124036)
- Ng T.H.; Chim W.K.; Choi W.K.; Ho V.; Teo L.W.; Du A.Y.; Tung C.H.; *Appl. Phys. Lett.* **2004**, *84*, 4385.
DOI: [10.1063/1.1757022](https://doi.org/10.1063/1.1757022)
- Wang S.; Liu W.; Wan Q.; Dai J. Y.; Lee P. F.; Suhua L.; Shen Q.; Zhang M.; Song Z.; and Lin C.; *Appl. Phys. Lett.* **2005**, *86*, 113105.
DOI: [10.1063/1.1864254](https://doi.org/10.1063/1.1864254)
- Hanafi H. I.; Tiwari S.; Khan I.; *IEEE Trans Electron Devices* **1996**, *43*, 1553.
DOI: [10.1109/16.535349](https://doi.org/10.1109/16.535349)
- Kim J K.; Cheong H J.; Kim Y.; Yi J Y.; Bark H J.; Bang S H.; Cho J H.; *Appl Phys Lett.* **2003**, *82*, 2527.
DOI: [10.1063/1.1567039](https://doi.org/10.1063/1.1567039)
- Blauwe J.; *IEEE Trans Nanotechnol* **2002**, *1*, 72.
DOI: [10.1109/TNANO.2002.1005428](https://doi.org/10.1109/TNANO.2002.1005428)
- Hori T, Ohzone T, Odark Y and Hirase J *IEEE IEDM Tech. Dig.* **1992**, *92*, 469.
DOI: [10.1109/IEDM.1992.307403](https://doi.org/10.1109/IEDM.1992.307403)
- Das K.; Goswami M N.; Mahapatra R.; Kar G S.; Dhar A.; Acharya H N.; Maikap S.; Lee J H.; Ray S. K.; *Appl. Phys. Lett.* **2004**, *84*, 1386.
DOI: [10.1063/1.1646750](https://doi.org/10.1063/1.1646750)
- Kim D W.; Kim T.; Banerjee S K.; *IEEE Trans Electron Devices* **2003**, *50*, 1823.
DOI: [10.1109/TED.2003.815370](https://doi.org/10.1109/TED.2003.815370)
- Tan Z.; Samanta S K.; Yoo W J.; Lee S.; *Appl Phys Lett.* **2007**, *86*, 013107.
DOI: [10.1063/1.1846952](https://doi.org/10.1063/1.1846952)
- Mikhelashvili V.; Meyler B.; Yoffis S.; Salzman J.; Garbrecht M.; Cohen-Hyams T.; Kaplan W. D.; and Eisenstein G.; *Applied Physics Letters* **2009**, *95*, 023104.
DOI: [10.1063/1.3176411](https://doi.org/10.1063/1.3176411)
- Wang Q.; Songa Z T.; Liua W L.; Lina C L.; Wang T H.; *Applied Surface Science.* **2004**, *230*, 8.
DOI: [10.1016/j.apsusc.2004.02.045](https://doi.org/10.1016/j.apsusc.2004.02.045)
- Singha A.; Roy A.; Kabiraj D.; and Kanjilal D.; *Semicond. Sci. Technol.* **2006**, *21*, 1691.
DOI: [10.1088/0268-1242/21/12/032](https://doi.org/10.1088/0268-1242/21/12/032)
- Maeda Y.; *Phys. Rev. B* **1995**, *51*, 1658.
DOI: [10.1103/PhysRevB.51.1658](https://doi.org/10.1103/PhysRevB.51.1658)
- Park C J.; Cho K H.; Yang W C.; Cho H Y.; Choi S H.; Elliman R G.; Han J H.; and Kim C.; *Appl. Phys. Lett.* **2006**, *88*, 071916.
DOI: [10.1063/1.2175495](https://doi.org/10.1063/1.2175495)
- Rao N. S.; Pathak A P.; Kulriya P. K.; Sathish N.; Devaraju G.; Agarwal D. C.; Saravanan G. S.; Saikiran V.; Avasthi D. K.; *Solid State Communications* **2010**, *150*, 2122.
DOI: [10.1016/j.ssc.2010.09.014](https://doi.org/10.1016/j.ssc.2010.09.014)
- Beyer A, Leifeld O, Muller E, Stutz S, Sigg H and Grutzmacher D *Thin Solid Films* **2000**, *380*, 246.
DOI: [10.1016/S0040-6090\(00\)01516-9](https://doi.org/10.1016/S0040-6090(00)01516-9)
- Boscherini F.; Capellini G.; Gaspare L. D.; Seta M. D.; Rosei F.; Sgarlata A.; Motta N.; Mobilio S.; *Thin Solid Films* **2000**, *380*, 173.
DOI: [10.1016/S0040-6090\(00\)01496-6](https://doi.org/10.1016/S0040-6090(00)01496-6)
- Desnicaa U. V.; Buljana M.; Dubceka P.; Siketica Z.; Radovica I. B.; Bernstorff S.; Serincanc U.; Turanc R.; *Nucl. Inst. and Meth. in Res. B* **2006**, *249*, 843.
DOI: [10.1016/j.nimb.2006.03.151](https://doi.org/10.1016/j.nimb.2006.03.151)
- Das S.; Singha R. K.; Manna S.; Gangopadhyay S.; Dhar A.; Pavesi L.; Ray S. K.; *J Nanopart Res.* **2001**, *13*, 587.
DOI: [10.1186/1556-276X-7-143](https://doi.org/10.1186/1556-276X-7-143)
- Das S.; Singha R. K.; Gangopadhyay S.; Dhar A.; Ray S. K.; *J. Appl. Phys.* **2010**, *108*, 053510.
DOI: [10.1063/1.3475717](https://doi.org/10.1063/1.3475717)
- Das S.; Das K.; Singha R. K.; Dhar A.; Ray S. K.; *Appl Phys Lett* **2007**, *91*, 233118.

- DOI: [10.1063/1.2821114](https://doi.org/10.1063/1.2821114)
24. Serincan U.; Kartopu G.; Guennes A.; Finstad T. G.; Turan R.; Ekinci Y.; Bayliss S. C.; *Semicond. Sc. Technol.* **2004**, *19*, 247.
DOI: [10.1088/0268-1242/19/2/021](https://doi.org/10.1088/0268-1242/19/2/021)
25. Duguay S.; Grob J. J.; Slaoui A.; Gall Y. Le.; and Amann-Liess M.; *J. Appl. Phys.* **2005** *97*, 104330.
DOI: [10.1063/1.1909286](https://doi.org/10.1063/1.1909286)
26. Som T.; Satpati B.; Prokert F.; Cantelli V.; and Kabiraj D.; *Nanotechnology* **2006**, *17*, 5248.
DOI: [10.1088/0957-4484/17/20/034](https://doi.org/10.1088/0957-4484/17/20/034)
27. Som T.; Satpati B.; Satyam P. V.; Kabiraj D.; Gupta A.; and Mishra N C.; *Journal of Applied Physics* **2004**, *96*, 7141.
DOI: [10.1063/1.1812819](https://doi.org/10.1063/1.1812819)
28. Saikiran V.; Rao N. S.; Devaraju G.; and Pathak A P.; *Nucl. Inst. Meth B.* **2014**, *323*, 14-18.
DOI: [10.1016/j.nimb.2014.01.004](https://doi.org/10.1016/j.nimb.2014.01.004)
29. Saikiran V.; Rao N. S.; Devaraju G.; Chang G. S.; and Pathak A. P.; *Nucl. Inst. Meth B* **2013**, *315*, 161.
DOI: [10.1016/j.nimb.2013.04.008](https://doi.org/10.1016/j.nimb.2013.04.008)
30. Saikiran V.; Vendamani V. S.; Hamad S.; Nageswara Rao S V S.; Rao S V.; and Pathak V.; *Nucl. Inst. Meth B* **2014**, *333*, 99.
DOI: [10.1016/j.nimb.2014.04.013](https://doi.org/10.1016/j.nimb.2014.04.013)
31. Carrada M.; Sahu B. S.; Bonafos C.; Gloux.; Groenen J.; Muller D.; Slaoui A.; *Thin Solid Films* **2013**, *543*, 94.
DOI: [10.1016/j.tsf.2013.02.113](https://doi.org/10.1016/j.tsf.2013.02.113)
32. Sahu B. S.; Gloux F.; Slaoui A.; Carrada M.; Muller D.; Groenen J.; Bonafos C.; Lhostis S.; *Nanoscale Research Letters* **2011**, *6*, 177.
DOI: [10.1186/1556-276X-6-177](https://doi.org/10.1186/1556-276X-6-177)
33. Saikiran V.; Rao N. S.; Devaraju G.; Chang G. S.; and Pathak A. P.; *Nucl. Inst. Meth B* **2013**, *312*, 1.
DOI: [10.1016/j.nimb.2013.07.005](https://doi.org/10.1016/j.nimb.2013.07.005)
34. Campbell I. H., and Fauchet, P. M. *Solid State Commun.* **1986**, *58*, 739.
DOI: [10.1016/0038-1098\(86\)90513-2](https://doi.org/10.1016/0038-1098(86)90513-2)
35. Zi, J., Zhang, K., Xie X. *Phys. Rev. B* **1999**, *55*, 9263.
DOI: [10.1103/PhysRevB.55.9263](https://doi.org/10.1103/PhysRevB.55.9263)
36. S. Vadavalli, S. Valligatla, B. Neelamraju, M. H. Dar, A. Chiasera, M. Ferrari and N. R. Desai *Front. Phys.* **2014**, *2*, 57.
DOI: [10.3389/fphy.2014.00057](https://doi.org/10.3389/fphy.2014.00057)
37. Toulemonde M.; Dufour, C.; Paumier, E.; *Phys. Rev. B* **1992**, *46*, 14362.
DOI: [10.1103/PhysRevB.46.14362](https://doi.org/10.1103/PhysRevB.46.14362)
38. Rui W.; Zhou B.; Li Q.; Jiang Z. Y.; Bo W.; Ma W. Y.; and Zhang X. D.; *J. Phys. D: Appl. Phys.* **2012**, *45*, 125304.
DOI: [10.1088/0022-3727/45/12/125304](https://doi.org/10.1088/0022-3727/45/12/125304)
39. Rao N. S.; Dhamodaran S.; Pathak A. P.; Kulriya P. K.; Mishra Y K.; Singh F.; Kabiraj D.; Pivin J. C.; Aasthi D. K.; *Nucl. Inst. Meth B* **2007**, *264*, 249.
DOI: [10.1016/j.nimb.2007.08.094](https://doi.org/10.1016/j.nimb.2007.08.094)
40. Goswami D. K.; and Dev B. N.; *Phys. Rev. B* **2003**, *68*, 033401.
DOI: [10.1103/PhysRevB.68.033401](https://doi.org/10.1103/PhysRevB.68.033401)
41. Zhou H.; Zhou L.; Özaydin G.; Ludwig K F.; and Headrick R L.; *Phys. Rev. B* **2008**, *78*, 165404.
DOI: [10.1103/PhysRevB.78.165404](https://doi.org/10.1103/PhysRevB.78.165404)
42. Frost, F.; Ziberi B.; Schindler A.; Rauschenbach B.; *Appl. Phys. A* **2008**, *91*, 551.
DOI: [10.1007/s00339-008-4516-0](https://doi.org/10.1007/s00339-008-4516-0)



A Monthly Journal

Publish your article in this journal

Advanced Materials Letters is an official international journal of International Association of Advanced Materials (IAAM, www.iaamonline.org) published monthly by VBRI Press AB from Sweden. The journal is intended to provide high-quality peer-review articles in the fascinating field of materials science and technology particularly in the area of structure, synthesis and processing, characterisation, advanced-state properties and applications of materials. All published articles are indexed in various databases and are available download for free. The manuscript management system is completely electronic and has fast and fair peer-review process. The journal includes review article, research article, notes, letter to editor and short communications.

www.vbripress.com/aml

Copyright © 2016 VBRI Press AB, Sweden